

# An optimum design for steel fiber reinforced concretes under cyclic loading

F. Bayramov, T. Aydoner, A. Ilki, C. Tasdemir & M.A. Tasdemir  
*Istanbul Technical University, Maslak, Istanbul, Turkey*

**ABSTRACT:** In this research, combined effects of the aspect ratio and volume fraction of steel fibers on the mechanical and fracture properties of Steel Fiber Reinforced Concretes (SFRCs) under cyclic loading were investigated using the three point bending test. Then, the fracture parameters of SFRCs were optimized to obtain the most economical mixture which also behaves in a relatively more ductile manner. For optimization, three-level full factorial experimental design, Response Surface Method and a multi-objective simultaneous optimization technique containing desirability functions were used.

**Keywords:** steel fiber reinforced concrete, cyclic loading, fracture energy, multi-objective optimization

## 1 INTRODUCTION

Steel Fiber Reinforced Concrete (SFRC) is a composite material consisting of concrete with steel fibers. SFRCs can be used when high tensile strength and reduced cracking are required, or even when conventional reinforcement can not be placed because of the shape of structural member. These composite materials are produced by using the same concrete constituents used in ordinary concrete (i.e. fine and coarse aggregates, cement, water, with or without mineral (or/and chemical) admixtures), and steel fibers. The fracture energy ( $G_F$ ) of these materials can reach up to about 300 times that of normal strength concrete or even 1350 times for SIFCON (Slurry Infiltrated Fibered Concrete). Since these materials have excellent impact resistance properties depending on their applications, conventional SFRCs or high performance SFRCs can be employed for, i) industrial floors, ii) concrete roads exposed to heavy traffic, iii) military structures, iv) strategically important structures in case of earthquake, v) some structures for industrial waste materials, vi) retrofitting of reinforced concrete structures, vii) small or medium size prefabricated elements (Bayramov et al. 2003). Three decades of research has enabled the production of SFRCs with good strength, stiffness, crack control, toughness and energy absorption capacity (Lee et al. 2003).

Until recently, the optimization of SFRCs has been generally made by maximizing the fracture energy. Li et al. (1991) solved what was essentially an optimization problem and also obtained approximate optimal values of fiber aspect ratio and the frictional bond strength between the fiber and matrix by first relating the objective function  $G_F$  to these fiber parameters. In another work, Brandt (1995) addressed to the issues about the simultaneous maximization of  $G_F$ , compressive strength ( $f_c'$ ), and the first cracking strength of FRC. These objective functions were related empirically to the mix, and the fiber variables. Lange-Kornbak & Karihaloo (1998) were the first to use mathematical optimization techniques for the maximization of  $G_F$  and  $f_c'$  (either separately or simultaneously) of SFRC. They developed rigorous micromechanical relations between tensile strength and fracture energy, and the mix and fiber parameters.

In SFRCs, the important parameters are the aspect ratio ( $L/d = \text{length/diameter}$ ) and volume fraction of fiber ( $V_f$ ). The main objective of this work is to determine strength and fracture properties to obtain a more ductile behavior than that of plain concrete. At the mean time, fracture parameters of various SFRCs were optimized.

In this study, a multi-objective simultaneous optimization technique is used to optimize SFRC with special emphasis on ductility, in which

Response Surface Method (RSM) is incorporated. RSM, has been widely used to optimize products and processes in manufacturing, chemical and other industries, but it has had limited use in the concrete industry. In one study, Simon et al. (1999) optimized High Performance Concrete mixtures using this method. The use of RSM to optimize SFRC mix design variables can significantly increase not only characteristic length ( $l_{ch}$ ), but also splitting tensile strength ( $f_{st}$ ) and flexural strength ( $f_{flex}$ ).

## 2 EXPERIMENTAL WORK

### 2.1 Mixes

Nine SFRC mixes and a plain (control) concrete mix were cast for this investigation. In all the mixes, the volume fractions of cement, siliceous sand, limestone fines, crushed limestone, and water were kept constant. Water to cement ratio was 0.36. Cement used was ordinary Portland cement with a density of  $3.16 \text{ g/cm}^3$  and the cement content of concrete was  $400 \text{ kg/m}^3$ . Siliceous sand (0-0.25mm) and limestone fines (0-4mm) were used as fine aggregates; their densities were  $2.63$  and  $2.65 \text{ g/cm}^3$ , respectively. As coarse aggregate, crushed limestone was used. The maximum particle size of aggregate was 16mm. The density of coarse aggregate was  $2.65 \text{ g/cm}^3$ . The amount of high-range water reducing admixture varied between 0.75% and 1.5% by weight of cement for different concrete mixtures to maintain sufficient workability. The volume fractions of steel fibers were 0.26 %, 0.45 %, and 0.64 %, and the aspect ratios of fibers were 55, 65, and 80.

In mixing, cement, siliceous sand, limestone fines and crushed limestone were blended first and then, high-range water reducing admixture and water were added to the mix. Steel fibers were scattered on the mixture and carefully mixed to achieve a uniform distribution of the fibers in the concrete.

The specimens were cast in steel moulds and compacted on a vibration table. All the specimens were demoulded after about 24 hours, stored in water saturated with lime, at  $20^\circ\text{C}$  until 28 days of age. At least 3 specimens of each concrete mix were tested under each type of loading condition at the 28th day. The beams prepared for the fracture energy tests were 500 mm in length and 100x100mm in cross section. Three cylinders 150 mm in diameter and 300 mm in height were used for compressive tests; and for the splitting test, six disc specimens 150 mm in diameter and 60 mm in height were prepared.

### 2.2 Test Procedure

Standard strength tests were conducted in accordance with European Standards (EN 206 and EN 12390). For all the beams, the tests for the determination of the fracture energy ( $G_F$ ) were performed according to the recommendation of RILEM 50-FMC Technical Committee (1985). Since the ratio of compressive strength to tensile strength of the SFRC tested in this work is in the range of 5 to 10, the method suggested by Hillerborg (1983) and also pointed out by Barros & Figueiras (1999) has been used. The effective cross section, however, was reduced to 60x100mm by sawing in order to accommodate both large aggregates and steel fibers used. The notched beam specimen tested is shown in Figure 1. SFRC beam specimens were tested at the loading rate of 0.3 mm/min up to a deflection of 2 mm, and then at 1.5 mm/min up to a 5 mm deflection. As schematically seen in Figure 1, the deflections were measured simultaneously by using two linear variable displacement transducers (LVDTs). The load was applied by an MTS actuator of 250 kN maximum capacity. The load versus midspan deflection curve for each specimen was obtained by recording the average of two measurements taken at the midspan.

The load-deflection curves were used for evaluating the fracture energy. The area under the load versus deflection at midspan curve ( $W_0$ ) was described as a measure of the fracture energy of the material (Fig. 1b).

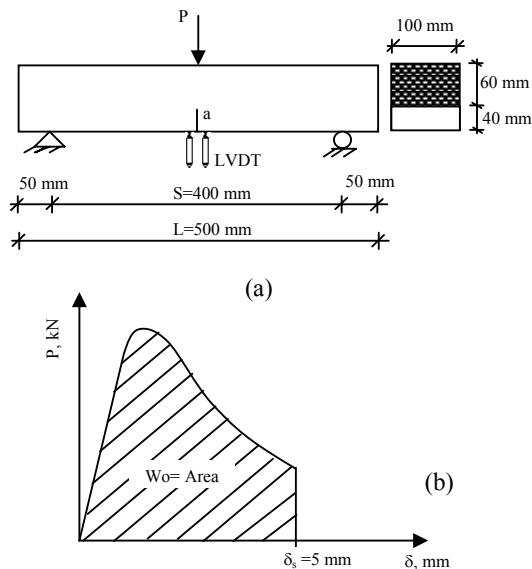


Figure 1. Schematic representation of the test setup (a), and the evaluation of fracture energy (b).

The results obtained here are based on the area under the complete load-deflection curve up to a specified deflection. This cut-off point was chosen as 5mm deflection. It is seen from the schematic curve that, the energy at this specified deflection (i.e. 5mm), however, is not totally dissipated. As shown in Figure 1, this property was determined using the following expression (RILEM 1985):

$$G_F = \frac{W_0 + mg \frac{S}{L} \delta_s}{B(D-a)} \quad (1)$$

Here, B, D, a, S, L, and m are the width, depth, notch depth, span, length, and mass of the beam, respectively.  $W_0$  is the area under the load-midspan deflection curve. g is the gravitational acceleration and  $\delta_s$  is the specified deflection of the beam.

### 3 EXPERIMENTAL RESULTS

#### 3.1 Strength properties

Compressive strength test results obtained from cylinder specimens are given in Table 1. The effect of the volume fraction of steel fiber seems to be more significant in concretes with the aspect ratio of 65. An increase in the fiber volume fraction ( $V_f$ ) from 0.26 % to 0.64 % has resulted in an increase of 30 % in the compressive strength. However, for the aspect ratio of 55 and 80, no significant change occurs when the fiber volume fraction is increased; thus the effect of the volume fraction of steel fiber on compressive strength is not consistent. However, the diameter of the steel fiber and possibly the orientation may have played an important role in compression. On the other hand, the addition of steel fibers into concrete may have an effect of increasing the ductility in the compressive failure rather than the compressive strength itself.

There is no significant effect of fiber volume fraction on the modulus of elasticity.

Tensile strength values evaluated from splitting tests on disc specimens are included in Table 1. It

is seen that the splitting tensile strength increases with increasing steel fiber volume fraction. For the fiber aspect ratio of 55, an increase of the fiber volume fraction from 0 (i.e. normal concrete) to 0.64 % has resulted in an increase of 23% in corresponding splitting tensile strength. For the aspect ratios of 65 and 80, this increase was 42% and 24%, respectively. Thus, it can be concluded that more significant enhancements were obtained in SFRCs with the fiber aspect ratio of 65.

Along the fracture plane, the opening and propagation of the crack are controlled by the steel fibers. During the crack propagation some fibers are broken but some of them are pulled-out of the matrix. After completion of the splitting tests the fracture surfaces were examined. In most cases, the fibers with the aspect ratio of 65 ( $L/d=65$ ) were not broken but were pulled out of the matrix. However, the fibers with the aspect ratio of 80 ( $L/d=80$ ) were broken into two parts. The results obtained for the fibers with  $L/d=65$  might be due to their larger cross sections compared to that of fibers with  $L/d=80$ . Similar results were obtained by Eren & Çelik (1997). The cylinder compressive strength of plain concrete used in this study is about 60 MPa, so for the steel fibers of  $L/d=80$ , the mechanical mismatch between steel fibers and concrete may have also played a role in this behavior. In this study, tensile strength of steel fibers used was 1100 MPa. For high strength concretes, however, high strength steel fiber with a tensile strength of 2000 MPa is suggested (Vandewalle 1996, Grünewald & Walraven 2002).

Flexural strengths of notched beams subjected to three-point bending tests are given in Table 1. The table shows that flexural strength increases as the fiber volume fraction increases. For the fiber aspect ratio of 55, an increase in the fiber volume fraction from 0 (i.e. normal concrete) to 0.64 %, has resulted in an increase of 33.5% in flexural strength. For the fiber aspect ratios of 65 and 80, the increases were 56.5% and 100%, respectively. The fracture process of steel fiber reinforced concrete consists of progressive debonding of fiber,

Table 1. Strength and fracture properties of concrete tested.

Fiber aspect ratio (L/d)	-	55			65			80		
		0.26	0.45	0.64	0.26	0.45	0.64	0.26	0.45	0.64
Fiber volume fraction ( $V_f$ ), %	0	0.26	0.45	0.64	0.26	0.45	0.64	0.26	0.45	0.64
Compressive strength ( $f_c'$ ), MPa	60.5	46.1	48.4	45.4	57.3	69.3	74.4	51.4	54.3	55.4
Flexural strength ( $f_{flex}$ ), MPa	6.1	6.04	7.0	8.1	6.7	6.9	9.5	6.4	7.3	12.1
Splitting tensile strength ( $f_a$ ), MPa	5.3	5.6	5.71	6.52	6.36	6.83	7.55	5.92	5.95	6.58
Modulus of elasticity (E), GPa	52.2	49.7	46.7	44.6	51.7	49.5	49.1	45.4	46.4	48.1
Fracture energy ( $G_F$ ), N/m	91	1011	1851	3368	957	1939	3724	1024	1793	4371
Characteristic length ( $l_{ch}$ ), mm	169	1599	2650	3537	1224	2056	3207	1327	2352	4845

during which slow crack propagation occurs. Final failure occurs due to unstable crack propagation when the fibers are pulled out and the interfacial shear stress reaches the ultimate strength. The reason for the increase in flexural strength is that, after matrix cracking, fibers carry the load subjected to concrete until the cracking of interfacial bond between fibers and matrix occurs. At higher aspect ratios, the advantage of using fibers for increasing flexural strength of concrete seems to be more significant (Gao et al. 1997).

### 3.2 Fracture properties

Specific fracture energy ( $G_F$ ) values of the mixes are given in Table 1. It can clearly be seen that specific fracture energy increases as the fiber volume fraction increases. These SFRCs allow obtaining high values of specific fracture energies and as a result a high ductility; depending on their aspect ratios and volume fractions of fibers used. The ductility is more than about 40 times greater than that of normal concrete. The increase in the specific fracture energy is because of the high energy of fiber pull-out and fiber debonding in the fracture process. The reason for the increase in specific fracture energy with increasing fiber volume fraction and its aspect ratio stems from a great number of fibers forming a bridge in the crack forming tortuous crack propagation.

In order to obtain the ductility of the mixes, characteristic length ( $l_{ch}$ ) was calculated using the measured specific fracture energy ( $G_F$ ), modulus of elasticity ( $E$ ), and direct tensile strength ( $f_t'$ ) according to the following expression introduced in the Fictitious Crack Model by Hillerborg (1976):

$$l_{ch} = \frac{G_F E}{f_t'^2} \quad (2)$$

In this study, the direct tensile strength ( $f_t'$ ) term in this relation was replaced by splitting tensile strength ( $f_{st}$ ). As seen in Table 1, as both aspect ratio and volume fraction of the steel fiber increase, the characteristic length increases significantly. Hence, it can be concluded that the results obtained give a clear picture of how a quasi-brittle concrete transforms into a ductile composite with the addition of steel fibers.

### 3.3 Degradation properties

The determination of a unique focal point of stiffness degradation in concrete has been defined by Lee et al. (1995) for compression, and used by Tasdemir et al. (1999) for three point bending, as

shown in Figure 2. In the later one, the first three unloading-reloading cycles has been used to locate the focal point; when the postpeak load dropped to about 40 percent of the maximum value, further cycles proved to be inappropriate to use. The normalized stiffness as a measure of degradation of stiffness and the focal point had been determined by Tasdemir et al. (1999) using unloading-reloading cycles, in both the load-Crack Mouth Opening Displacement (CMOD) and the load-deflection curve. The normalized stiffness had been correlated to the normalized local fracture energy, to the normalized permanent CMOD and  $\delta$ , and the normalized load (strength degradation). In the later one, the focal point has been employed as a measure of concrete brittleness. Depending on the type of aggregate and silica fume, the ranges of the coordinates of focal point were: -0.019 mm to -0.089 mm for  $\delta_0$ , and -0.78 kN to -1.47 kN for  $P_0$ .

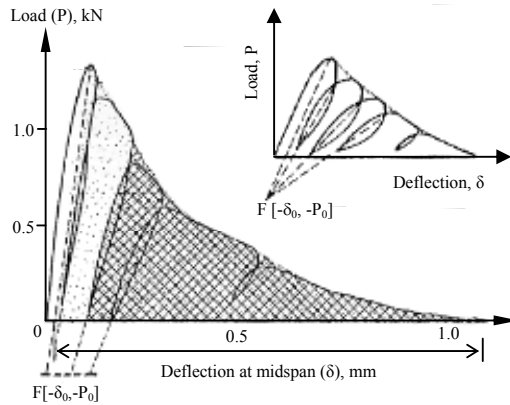


Figure 2. Typical results of unloading-reloading cycles for a plain concrete beam (Tasdemir et al. 1999).

Figures 3-5 show load-midspan deflection curves obtained from the bending tests on SFRC beams in cases of different fiber aspect ratios and volume fractions. Under cyclic actions steel fibers efficiently bridge the cracks and no significant loss of stiffness is observed even when high levels of deflections are reached. Similar results were obtained by Campione et al. (2001). In this work, the first two unloading-reloading cycles were used to determine the focal point. As seen in these figures, especially for high volume fractions of steel fiber there is no significant loss in the initial compliance, i.e. in SFRCs the slopes of the unloading-reloading loops are almost same as the slope of the initial ascending part of the load-deflection curve. Depending on the steel fiber volume fraction ( $V_f$ ) and the aspect ratio ( $L/d$ ),

coordinates of focal point can reach up to (-11.0 mm, -78.5 kN). This is an evidence of the ductility of SFRCs. Although, the residual strength decreases after the peak stress, stiffness degradation in SFRCs is not significant.

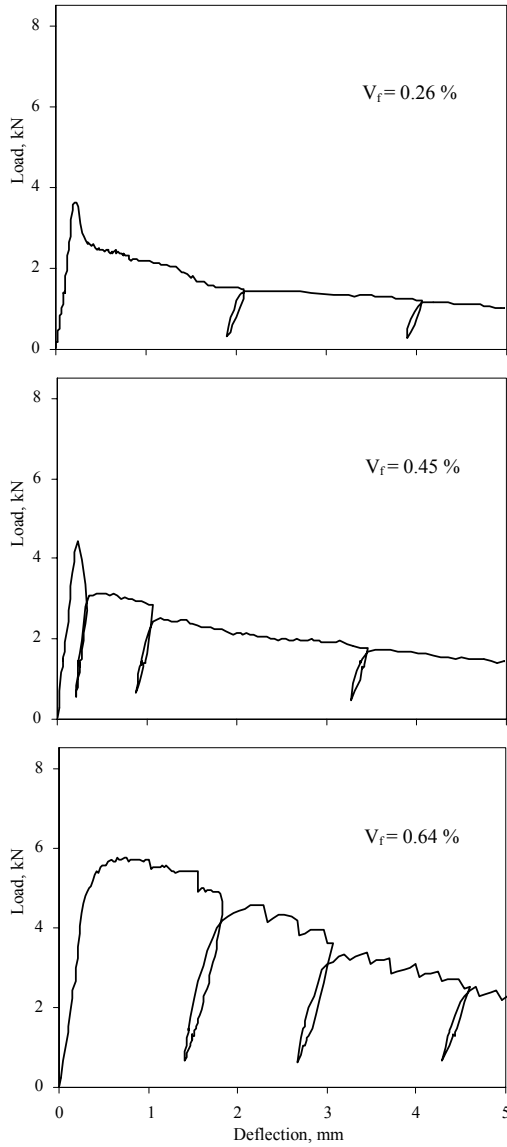


Figure 3. Typical load-midspan deflection curves of SFRCs with the fiber aspect ratio of 55.

#### 4 OPTIMUM DESIGN

In this study, a multi-objective simultaneous optimization technique is used to optimize SFRC

with special emphasis on ductility, in which Response Surface Method (RSM) is incorporated. To optimize a process or to find the best-fitting function of a number of experimental points, a model has to be found first; after this, the optimization procedure is performed using the response surface of the model as the basis for finding the best solution.

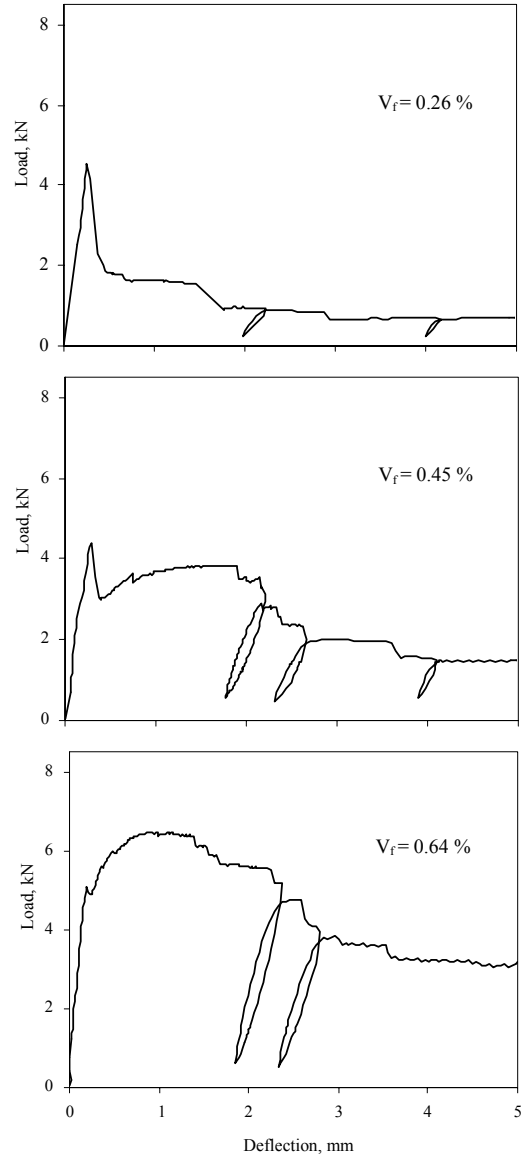


Figure 4. Typical load-midspan deflection curves of SFRCs with the fiber aspect ratio of 65.

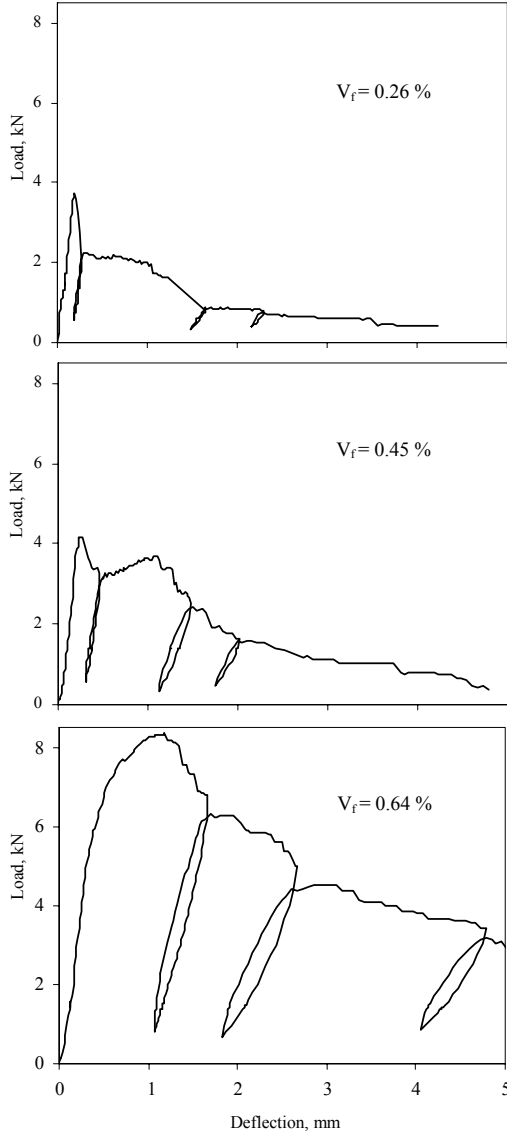


Figure 5. Typical load-midspan deflection curves of SFRCs with the fiber aspect ratio of 80.

A common response surface experimental plan which can be used to find optimal settings is a two variable (i.e.  $L/d$  and  $V_f$ ), three-level (i.e.  $L/d=55, 65,$  and  $80$ ;  $V_f=20 \text{ kg/m}^3, 35 \text{ kg/m}^3,$  and  $50 \text{ kg/m}^3$ ) full factorial experimental design. The full factorial design for two independent variables consists of  $3^2=9$  mixes.

Nine experimental data for each response of SFRCs shown in Table 1, were fitted to a polynomial type of mathematical model by using analysis of variance (ANOVA) and by adjusting

parameters until calculated values were in close agreement with the experimental values. For each mechanical and fracture property of SFRCs the fitted regression models are given below (Bayramov et al. 2003):

$$G_F = 3542.1 - 33.64(L/d) - 11514V_f + 13468.16V_f^2 + 103.41(L/d)V_f \quad (3)$$

$$f'_c = -530.12 + 17.26 (L/d) + 17.75 V_f - 0.13(L/d)^2 \quad (4)$$

$$f_{st} = -21.68 + 0.84 (L/d) - 2.91 V_f - 0.01 (L/d)^2 + 5.98 V_f^2 \quad (5)$$

$$E = -15.89 + 2.48 (L/d) - 74.42 V_f - 0.02 (L/d)^2 + 17.15 V_f^2 + 0.82 (L/d) V_f \quad (6)$$

$$f_{flex} = 16.67 - 0.12 (L/d) - 44.64 V_f + 30.22 V_f^2 + 0.4 (L/d) V_f \quad (7)$$

$$I_{ch} = 21687.6 - 600.43 (L/d) - 5080.32 V_f + 3.95 (L/d)^2 + 173.53 (L/d) V_f \quad (8)$$

After building the regression model and establishing relationships between mix design variables and the responses expressed in Equations 3-8, all independent variables are varied simultaneously and independently in order to optimize the objective functions. The objective of optimization is to find the “best settings” that maximize a particular response or responses. Optimization usually involves considering several responses simultaneously. A numerical optimization technique using desirability functions ( $d_j$ ), which are defined for each response, can be used to optimize the responses simultaneously (Derringer & Suich 1980). A desirability function ( $d_j$ ) varies over the range of  $0 \leq d_j \leq 1$ . By using the single composite response ( $D$ ) given in Equation 10, which is the geometric mean of the individual desirability functions, the multi-objective optimization problem is solved.  $D$  is maximized over the feasible region of the design variables given in Equation 9 (Myers & Montgomery 2002):

$$55 \leq L/d \leq 80 \quad (9)$$

$$0.26\% \leq V_f \leq 0.64\%$$

$$D = (d_1 \times d_2 \times d_3 \times \dots \times d_n)^{\frac{1}{n}} \quad (10)$$

where  $n$  = the number of responses included in the optimization. If any of the responses or factors falls outside their desirability range, the overall function becomes zero.

In cases of the maximizing and minimizing of individual responses, the desirability functions ( $d_j$ ) defined by Derringer & Suich (1980) were employed. More details about these functions can be found in a previous work of the authors (Bayramov et al. 2003)

In this work, for building the regression model and optimization, a commercially available (Design-Expert) software package was used.

To attain a less brittle concrete, a concrete with the highest splitting tensile strength ( $f_{st}$ ), the highest characteristic length ( $l_{ch}$ ) and also the highest flexural strength ( $f_{flex}$ ) is to be obtained. So it is necessary to maximize  $f_{st}$ ,  $l_{ch}$  and  $f_{flex}$ , simultaneously. Thus, these three responses ( $f_{st}$ ,  $l_{ch}$  and  $f_{flex}$ ) are considered to be of equal importance (i.e. the weighting factor ( $w_{t_j}$ ) of the responses, equal to 1) and maximized simultaneously (Bayramov et al. 2003). For  $n=3$ , Equation 10 takes on the form:

$$D = (d_1 \times d_2 \times d_3)^{\frac{1}{3}} \quad (11)$$

where  $d_1$ ,  $d_2$  and  $d_3$  are the desirability functions of  $f_{st}$ ,  $l_{ch}$  and  $f_{flex}$ , respectively.

The solution of this multi-objective optimization is shown in Figure 6. The figure shows that, the optimal values of design variables are  $V_f = 0.64\%$  and  $L/d = 76.44$ . Since  $65 \leq L/d \leq 80$ , the limitations of  $L$  and  $d$  are:  $L = 60$  mm and  $0.75 \leq d \leq 0.92$  mm, thus  $L = 60$  mm and  $d = 0.785$  mm, which shows that  $d$  is between 0.75 and 0.92. The predicted response values and associated uncertainties (at 95% confidence level) are  $l_{ch} = 4068 \pm 415$  mm,  $f_{st} = 7.1 \pm 0.2$  MPa,  $f_{flex} = 11.3 \pm 0.7$  MPa,  $G_F = 4136 \pm 237$  N/m,  $E = 49.2 \pm 0.4$  GPa and  $f'_c = 65.7 \pm 4.7$  MPa.

The cost of the steel fibers used in the production of composites is also important when the application is of concern. Therefore, the volume fraction of steel fiber must be minimized to get an economical mixture. Numerical optimization can optimize any combination of either factors or responses. Thus,  $f_{st}$ ,  $l_{ch}$ ,  $f_{flex}$  and volume fraction of steel fiber ( $V_f$ ) are also considered to be of equal importance (i.e.  $w_{t_j} = 1$ ) and optimized simultaneously, i.e.  $f_{st}$ ,  $l_{ch}$  and  $f_{flex}$  are maximized and  $V_f$  is minimized. In this case Equation 10 takes on the form:

$$D = (d_1 \times d_2 \times d_3 \times d_4)^{\frac{1}{4}} \quad (12)$$

where  $d_1$ ,  $d_2$ ,  $d_3$ , and  $d_4$  are the desirability functions of  $f_{st}$ ,  $l_{ch}$ ,  $f_{flex}$  and  $V_f$ , respectively (Bayramov et al. 2003).

The solution of this multi-objective optimization is shown in Figure 7. This figure shows that, the optimal values of design variables are  $V_f = 0.56\%$  and  $L/d = 75.87$ , i.e.  $L = 60$  mm and  $d = 0.791$  mm. The predicted response values and associated uncertainties (at 95% confidence level) are  $l_{ch} = 3359 \pm 310$  mm,  $f_{st} = 6.8 \pm 0.1$  MPa,  $f_{flex} = 9.4 \pm 0.5$  MPa,  $G_F = 3125 \pm 165$  N/m,  $E = 48.6 \pm 0.3$  GPa and  $f'_c = 65 \pm 3.8$  MPa.

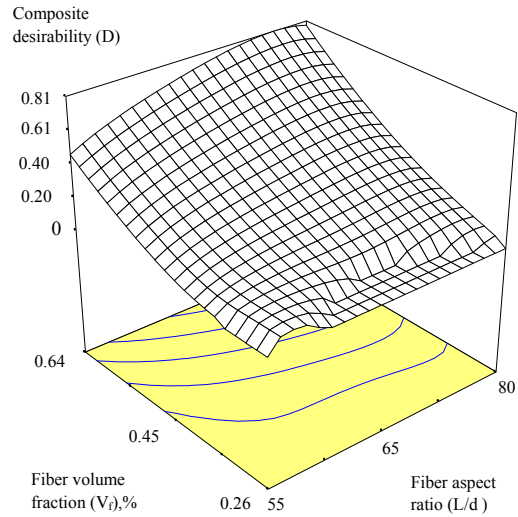


Figure 6. Response surface plot of the composite desirability (D) when  $f_{st}$ ,  $l_{ch}$  and  $f_{flex}$  are maximized simultaneously.

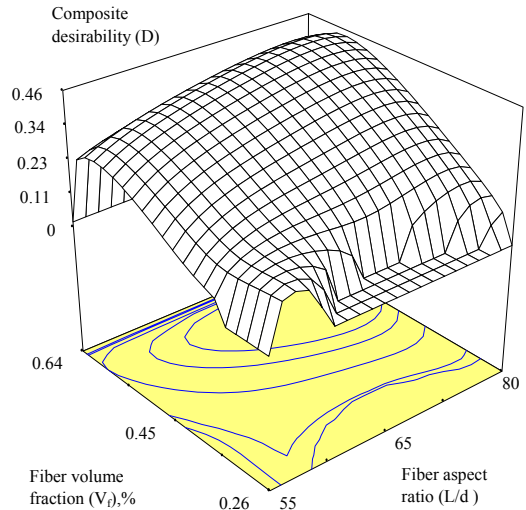


Figure 7. Response surface plot of the composite desirability (D) when  $f_{st}$ ,  $l_{ch}$  and  $f_{flex}$  are maximized and steel fiber volume fraction ( $V_f$ ) is minimized simultaneously.

## 5 CONCLUSIONS

The experimental design made by using response surface method provides a thorough examination of SFRC properties over the selected ranges of fiber volume fractions and aspect ratios. In order to provide an adequate representation of the responses, fitting quadratic models that are usually assumed to represent each concrete property of interest, can be done in identifying optimal mixes. The results show that the predictiveness of the polynomial regression model is satisfactory. The addition of steel fiber improves fracture properties significantly.

When the mechanical properties ( $f_{st}$ ,  $l_{ch}$  and  $f_{flex}$ ) are concerned, the optimal values of design variables obtained are as follows: a steel fibre volume fraction of 0.64 % and an aspect ratio of 76.44. For both mechanical properties ( $f_{st}$ ,  $l_{ch}$  and  $f_{flex}$ ) and cost optimization the optimal values of design variables obtained are as follows: a steel fiber volume fraction of 0.56 % and an aspect ratio of 75.87.

The focal point can be taken as a measure of concrete brittleness. In SFRCs, this point is far away from the origin compared to that of concretes without steel fibers. Although, the residual strength decreases gradually after the peak stress in SFRCs, the stiffness degradation is not significant under cyclic loading condition.

## ACKNOWLEDGEMENT

The financial support of TUBITAK (The Scientific and Technical Research Council of Turkey)-BAYG is greatly appreciated by the first author. The fourth and fifth authors wish to acknowledge the grant of The British Council (Britain-Turkey Partnership Program for the academic link between ITU and Cardiff University), and the financial supports of TUBITAK (Project: ICTAG 1665) and DPT (State Planning Organization, Project: 2002K120340). The support given by BEKSA is also gratefully acknowledged.

## REFERENCES

- Barros, J.A.O. & Figueiras, J.A. 1999. Flexural behavior of SFRC: Testing and modelling. *Journal of Materials in Civil Engineering* 11(4):331-339.
- Bayramov, F., Tasdemir, C. & Tasdemir, M.A. 2003. Optimisation of steel fibre reinforced concretes by means of statistical response surface method. *Cement and Concrete Composites*, in press.
- Brandt, A.M. 1995. *Cement-based composites: materials, mechanical properties and performance*. London: E & FN Spon.
- Campione, G., Miraglia, N. & Papia, M. 2001. Mechanical properties of steel fibre reinforced lightweight concrete with pumice stone or expanded clay aggregates. *Materials and Structures* 34: 201-210
- Derringer, G. & Suich, R. 1980. Simultaneous optimization of several response variables. *Journal of Quality Technology* 12(4): 214-219.
- Eren, Ö. & Çelik, T. 1997. Effect of silica fume and steel fibers on some properties of high-strength concrete. *Construction and Building Materials* 11(7-8): 373-382.
- Gao, J., Sun, W. & Morino, K. 1997. Mechanical properties of steel fibre-reinforced, high-strength, lightweight concrete. *Cement and Concrete Composites* 19: 307-313.
- Grünewald, S. & Walraven, J.C. 2002. High strength self-compacting fibre reinforced concrete: Behaviour in the fresh and hardened state. In *6th intern. symp. on HSC/HPC, eds., G König et al., Vol.2: 977-989, Leipzig, June 2002*.
- Hillerborg, A., Modeer, M. & Peterson, P.E. 1976. Analysis of crack formation and crack growths in concrete by means of fracture mechanics and finite elements. *Cement and Concrete Research* 6:773-782.
- Hillerborg, A. 1983. Concrete fracture energy tests performed by 9 laboratories according to a draft RILEM recommendation. *Rep. to RILEM TC 50-FMC, Rep. TVBM-3015, Lund Institute of Technology, Lund, Sweden*.
- Lange-Kornbak, D. & Karihaloo, B.L. 1998. Design of fibre-reinforced DSP mixes for minimum brittleness. *Advanced Cement Based Materials* 7: 89-101
- Lee, M.K., Lark, R.J. & Barr, B.I.G. 2003. A state of the art review on HPFRCC. *Report for Sub-task 15, Sustainable Advanced Materials for Road Infrastructure (SAMARIS)*.
- Lee, Y., Willam, K. & Kang, H.D. 1995. Experimental observations of concrete behavior under uniaxial compression. *Proceedings of FramCos-2, F.H. Wittmann eds., AEDIFICATIO publishers, Vol.1: 397-414, ETH Zurich, Switzerland, 25-28 July 1995*.
- Li, V.C., Wang, Y. & Backer, S.A. 1991. Micromechanical model of tension softening and bridging toughening of short random fibre reinforced brittle matrix composites. *Journal of Mechanics and Physics of Solids* 39: 607-625.
- Myers, R.H. & Montgomery, D.C. 2002. *Response surface methodology: process and product optimization using designed experiments*. New York: John Wiley & Sons.
- RILEM 50-FMC 1985. Committee of fracture mechanics of concrete. Determination of fracture energy of mortar and concrete by means of three-point bend tests on notched beams. *Materials and Structures* 18(106): 285-290.
- Simon, M.J., Lagergren, E.S. & Wathne, L.G. 1999. Optimizing high-performance concrete mixtures using statistical response surface methods. In *proc. of the 5th intern. symp. on utilization of high strength/high performance concrete, 1311-1321, Norwegian Concrete Association, Oslo, Norway*.
- Tasdemir, C., Tasdemir, M.A., Mills, N., Barr, B.I.G. & Lydon, F.D. 1999. Combined effects of silica fume, aggregate type, and size on post peak response of concrete in bending. *ACI Materials Journal* 96: 74-83.
- Vandewalle, L. 1996. Influence of the yield strength of steel fibres on the toughness of fibre reinforced high strength concrete. *Proc., the CCMS Symp., Worldwide Advances in Structural Concrete and Masonry, 496-505, Chicago*.